RESEARCH ARTICLE

Modeling and Control of a Brushless Multiphase Doubly-Fed Induction Generator in a Stand-Alone Wind Generation System

KRZYSZTOF BLECHARZ, ROLAND RYNDZIONEK, (Senior Member, IEEE), AND FILIP KUTT
Faculty of Electrical and Control Engineering, Gdańsk University of Technology, 80-233 Gdańsk, Poland
Corresponding author: Krzysztof Blecharz (krzysztof.blecharz@pg.edu.pl)

ABSTRACT The development of the novel multiphase brushless doubly-fed generator system and voltage controller for stand-alone mode configuration is proposed in this paper. The generator system is based on the new machine construction with multiphase control winding and traditional three-phase power winding. The dynamic model of multiphase brushless doubly-fed generator is presented, and the control strategy for voltage amplitude and frequency is developed. The simulation and experimental results are used to validate the performance of the topology of the multi-phase brushless double-fed generator and of the control system. The tests of the generator system have been carried out for the normal operating state of the system and for the case where one of the control phase is inactive. This situation is equivalent to a failure in the power path of the control winding.

INDEX TERMS Multiphase generator, brushless doubly-fed generator, vector control, stand-alone power generation, induction machine.

I. INTRODUCTION

The classic three-phase design of a brushless doubly-fed induction generator (BDFIG) has been well-known for many years [1], [2], [3], [4], [5]. These designs are promising as an alternative to the conventional slip-ring doubly-fed induction generator (DFIG) in variable-speed power generation applications. In the literature, a number of different topologies of the BDFIG have been reported, such as the brushless doubly-fed induction machine [6], [7], [8], [9], the cascade doubly-fed induction machine [10], the brushless reluctance doubly-fed generator [11], [12], and the dual-stator brushless doubly-fed generator [13], [14], [15]. BDFIG designs typically include two stator windings that are not directly coupled and rotor windings. The first winding, known as the power winding (PW), is a three-phase winding that can either be connected directly to the power grid or supply external load in stand-alone mode. The second winding, known as the control winding (CW), is also a

three-phase winding, but it is connected to a bidirectional voltage or current power converter [16], [17]. The third winding on the generator rotor provides the magnetic coupling between power and control windings. The rotor winding (RW) can be made in a fed-in winding or nested-loop configuration and various magnetic circuit configurations.

BDFIG is a promising wind energy generation technology with high reliability and low maintenance costs due to the lack of sliding contacts. In addition, manufacturing costs are expected to be lower than equivalent DFIGs [18], [19], [20]. This is due to the lack of a slip ring system and the simpler rotor winding design. Other positive features of this brushless generator include operation in a wide range of machine shaft speeds, which improves the efficiency of energy conversion; the power of the converter on the rotor side is about 30% of the total generator power; accurate control of active and reactive power; and good quality of power transmission to the grid. With so many benefits, it is important to understand their limitations. For instance, three-phase designs may not function correctly during a phase failure in the control winding. In a two-phase power supply case, the control

winding generates a flux that changes nature, leading to a loss of control over the generator. These factors should be taken into account when considering the implementation of BDFIGs. This disadvantage can be overcome by using multiphase control windings on the stator. In a five-phase system, even a two-phase failure does not change the rotating character of the magnetic field. Firstly, using five phases in the control winding while maintaining the three-phase structure of the power winding increases the reliability of the entire generator system while maintaining all technical advantages. Second, a more significant number of phases reduces CW harmonic currents by reducing the current level per phase and increasing the torque pulsation frequency while reducing its amplitude. The brushless multiphase doubly-fed induction generator (BMDFIG) configuration is shown in Figure 1.
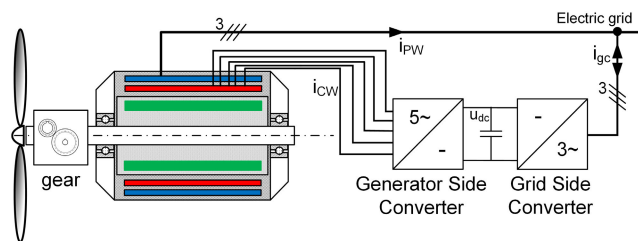

FIGURE 1. Configuration of brushless 5-phase doubly-fed generator.

The BMDFIG, similar to the BDFIG, can operate in grid and stand-alone modes. In stand-alone mode, the generator supplies an isolated variable load of various characters: resistive-inductive or resistive-capacitive. The main control objective is maintaining the power winding voltage and frequency independent of the generator load condition and the machine shaft speed. The control of the power winding voltages is achieved indirectly by controlling the current on the control winding. At the same time, the grid-isolated frequency is maintained by impressing proper slip-frequency currents from the control windings terminals. To achieve a high performance of the stand-alone generator system, it is necessary to use advanced control methods.

Besides different DFIG and BLDFIG topologies, different control strategy approaches have been described in literature. In [21] novel direct power control for open-winding for BLDFIG with dual two-level converter has been presented. The proposed system improve the fault tolerances and improve the voltage THD. However, the method requires much more transistors and complex control system. The [22] proposes the dual-resonant controller in generator side converter to achieve compensation when the system is under nonlinear or unbalanced loads. Moreover, the method can significantly reduce the numbers of PIR, P, and PI controllers. In [23] the efficiency improvement based on the loss analysis for both BDFIG and converter has been elaborate. The total system efficiency can be enhanced by 0.2–7.8% under the different operation conditions. As can be observed, research on BLDFIG is being conducted at various levels and with

diverse methodologies and approaches. In this article the study of the multiphase induction generator in terms of different phases in control winding is continued [24].

The main contributions of this paper are:
- Energy generation system based on a novel BMDFIG with improved the overall reliability;
- Mathematical model of the BMDFIG;
- Extends classic vector control with a dedicated and unique algorithm developed for the novel BMDFIG;
- Experimental validation of the proposed control strategy.

The structure of the paper is as follows: The mathematical model of the BMDFIG has been the subject of section II. Winding function approach and the FEA validation results have been presented in section III. The vector control of the stand-alone BMDFIG has been elaborated in section IV. The simulation and experimental analysis, including fault tolerance, are explained in Section IV. Finally, the paper summarizes the main conclusions

A. BMDFIG OPERATION

The BMDFIG can be used in two operation modes, synchronous and asynchronous modes, with cascade and induction configuration. If the CW is not directly connected to the power source or is short-circuited, the generator can operate in asynchronous induction or cascade modes. However, in both cases, it is necessary to provide capacitive reactive power from the network side to excite the machines. In both cases, the generator behaves like a classic squirrel-cage induction machine regarding generator operation. The general scheme of the generator is shown in Figure 2. In synchronous mode, the CW and PW are connected separately to two power sources, one directly to the grid and the other to a variable bidirectional voltage or current power converter source [25]. The synchronous speed in this operation mode is defined as

$$n_s = 60 \frac{(f_1 + f_2)}{p_1 + p_2} \tag{1}$$

where f_1 is the frequency of the power converter source, f_2 is the frequency of supplying the power winding from the power grid. The symbols p_1 and p_2 represent the number of pole pairs PW and CW, respectively. In synchronous mode, the generator works in an optimal regime and can be used in stand-alone applications when the grid voltage and frequency of the island grid are regulated and in grid configuration mode when active and reactive power transferred to the power grid is controlled.

The useful range for changing the shaft speed within the operating range of the machine's generator is a slip value of ± 0.3 around the synchronous speed. This is related to the rated power of the CW-powered converter.

II. MATHEMATICAL MODEL OF 5-PHASE BMDFIG
The BMDFIG is based on the BDFIG vector model [XX]. In this case, some assumptions have been taken into account:
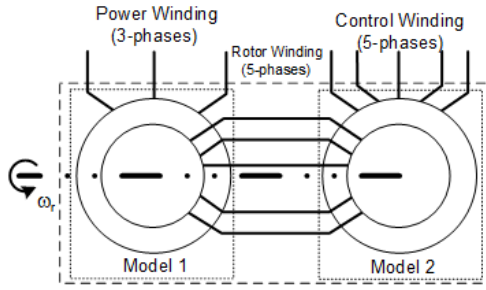
FIGURE 2. The general scheme of the BMDFIG.

FIGURE 3. Equivalent circuit of a BMDFIG for 1st and 2nd mathematical plane.

symmetrical distributed windings, uniform air gap, and sinusoidal MMF distribution. The BMDFIG has three sets of windings: 3-phase PW in the machine model equations marked as 1, 5-phase RW marked as ''r'', and 5-phase CW (instead of the 3-phase standard CW) marked as 2, respectively. The mathematical notation of a multiphase machine model in the form of differential equations in natural axes is of little use for applications in developing control systems. Therefore, after writing the equations of the machine model to an orthogonal system using the extended Clark transformation for five-phase systems, the generator model can be presented as a superposition of two systems described on two mathematical planes. The subscript (i = 1..2) defines the sets of state variable equations for two independent mathematical planes of state variables 1 and 2, where $R_{1(i)}$, $R_{r(i)}$, $R_{2(i)}$ and $L_{1(i)}$, $L_{r(i)}$, $L_{2(i)}$ are the PW, RW and CW parameters of resistance, inductances for different planes, respectively. The inductance matrices are the main difference between the multiphase generator model and a classic form of the BDFIG model. The mathematical model of the BMDFIG system can be determined using different reference frames, such as stationary $\omega_a = 0$ or any rotating frames, by applying the theory of space-rotating vectors for multiphase induction machines. The differential vector equations of the BMDFIG have a general form, which is as follows:

$$u_{1(i)} = \mathbf{R}_{1(i)}\mathbf{i}_{1(i)} + \frac{d\Psi_{1(i)}}{d\tau} + j\omega_a\Psi_{1(i)} \tag{2}$$

$$\mathbf{u}_{2(i)} = \mathbf{R}_{2(i)}\mathbf{i}_{2(i)} + \frac{d\Psi_{2(i)}}{d\tau} + j\left(\omega_a - (p_1 + p_2)\omega_{r(i)}\right)\Psi_{2(i)} \tag{3}$$

$$0 = \mathbf{R}_{r(i)}\mathbf{i}_{r(i)} + \frac{d\Psi_{r(i)}}{d\tau} + j\left(\omega_a - p_1\omega_{r(i)}\right)\Psi_{r(i)} \tag{4}$$

$$\Psi_{1(i)} = \mathbf{L}_{1(i)}\mathbf{i}_{1(i)} + \mathbf{L}_{m1(i)}\mathbf{i}_{r(i)} \tag{5}$$

$$\Psi_{2(i)} = \mathbf{L}_{2(i)}\mathbf{i}_{2(i)} + \mathbf{L}_{m2(i)}\mathbf{i}_{r(i)} \tag{6}$$

$$\Psi_{r(i)} = \mathbf{L}_{r(i)}\mathbf{i}_{r(i)} + \mathbf{L}_{m1(i)}\mathbf{i}_{1(i)} + \mathbf{L}_{m2(i)}\mathbf{i}_{2(i)} \tag{7}$$

$$J\frac{d\omega_r}{d\tau} = \frac{3}{2}p_1\text{Im}\left|\Psi_{1(i)}^*\ \mathbf{i}_{1(i)}\right| + \frac{5}{2}p_2\text{Im}\left|\Psi_2^{(i)}\ \mathbf{i}_{2(i)}^*\right| - T_{drive} \tag{8}$$

$$L_{1(1)} = \left(L_{\sigma 1(1)} + L_{1m}\right) \tag{9}$$

$$L_{2(1)} = \left(L_{\sigma 2(1)} + L_{2m}\right) \tag{10}$$

$$L_r = \left(L_{\sigma r(1)} + L_{1m} + L_{2m}\right) \tag{11}$$

where $\Psi_{1(i)}$, $\mathbf{i}_{1(i)}$, $\mathbf{u}_{1(i)}$ and $\Psi_{r(i)}$, $\mathbf{i}_{r(i)}$ and $\Psi_{2(i)}$, $\mathbf{i}_{2(i)}$, $\mathbf{u}_{2(i)}$ are the PW, RW and CW space vectors of magnetic fluxes,
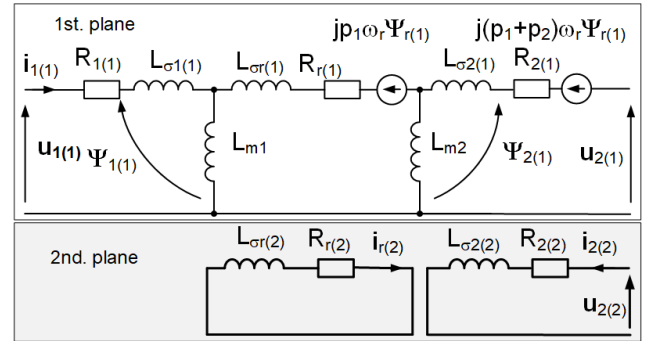
circuit currents and voltage for each mathematical plane, respectively.

The Figure 3 shows the equivalent diagram of the steady-state machine on the first and second mathematical planes. If the second mathematical plane is not considered, the diagram shown is identical to the classic generator design [26]. The mathematical model of stator-tied BMDFIG in the power winding reference frame is developed by considering the stationary reference frame. The vector components of the currents and fluxes of the generator state variables for the first mathematical plane are marked as $\alpha\beta$, respectively, and for the second one as xy. The model system of equations takes the following form for the first mathematical plane:

$$\frac{d\Psi_{1\alpha}}{d\tau} = -R_{1(1)}i_{1\alpha} + u_{1\alpha}$$

$$\frac{d\Psi_{1\beta}}{d\tau} = -R_{1(1)}i_{1\beta} + u_{1\beta} \tag{12}$$

$$\frac{d\Psi_{r\alpha}}{d\tau} = -R_{r(1)}i_{r\alpha} - p_1\omega_r\Psi_{r\beta}$$

$$\frac{d\Psi_{r\beta}}{d\tau} = -R_{r(1)}i_{r\beta} + p_1\omega_r\Psi_{r\alpha} \tag{13}$$

$$\frac{d\Psi_{2\alpha}}{d\tau} = -R_{2(1)}i_{2\alpha} - (p_1 + p_2)\omega_r\Psi_{2\beta} + u_{2\alpha}$$

$$\frac{d\Psi_{2\beta}}{d\tau} = -R_{2(1)}i_{2\beta} + (p_1 + p_2)\omega_r\Psi_{2\alpha} + u_{2\beta} \tag{14}$$

where vector components of flux linkages in (12)-(14) are defined as

$$\Psi_{1\alpha} = L_{1(1)}i_{1\alpha} + L_{1m}i_{r\alpha}$$

$$\Psi_{1\beta} = L_{1(1)}i_{1\beta} + L_{1m}i_{r\beta}$$

$$\Psi_{2\alpha} = L_{2(1)}i_{2\alpha} + L_{2m}i_{r\alpha}$$

$$\Psi_{2\beta} = L_{2(1)}i_{2\beta} + L_{2m}i_{r\beta}$$

$$\Psi_{r\alpha} = L_{r(1)}i_{r\alpha} + L_{1m}i_{1\alpha} + L_{2m}i_{2\alpha}$$

$$\Psi_{r\beta} = L_{r(1)}i_{r\beta} + L_{1m}i_{1\beta} + L_{2m}i_{2\beta} \tag{15}$$

The equations for the second mathematical plane are as follows:

$$\frac{d\Psi_{2x}}{d\tau} = -R_{2(2)}i_{2x} + u_{2x}$$

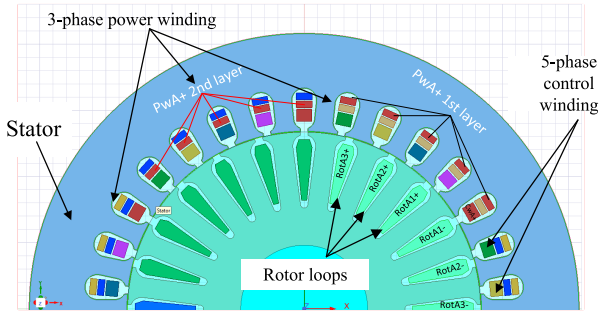$$\frac{d\Psi_{2y}}{d\tau} = -R_{2(2)}i_{2y} + u_{2x}$$

FIGURE 4. The BLDFIG simulation model.

$$\frac{d\Psi_{rx}}{d\tau} + R_{r(2)}i_{rx} = 0$$
$$\frac{d\Psi_{ry}}{d\tau} + R_{r(2)}i_{ry} = 0 \tag{16}$$

where vector components of flux linkages in (16) are defined as

$$\Psi_{2x} = L_{\sigma 2(2)}i_{2x}$$
$$\Psi_{2y} = L_{\sigma 2(2)}i_{2y}$$
$$\Psi_{rx} = L_{\sigma r(2)}i_{rx}$$
$$\Psi_{ry} = L_{\sigma r(2)}i_{ry} \tag{17}$$

and the electrical torque is

$$J\frac{d\omega_r}{d\tau} = \frac{3}{2}(\Psi_{1\alpha}i_{1\beta} - \Psi_{1\beta}i_{1\alpha}) + \frac{5}{2}(\Psi_{2\beta}i_{2\beta} - \Psi_{2\beta}i_{2\alpha}) - T_{drive} \tag{18}$$

III. DESIGN 5-PHASE BMDFIG

The BLDFIG generally consists of a stator with a power winding and a control winding, a wound rotor and a shaft. The 3-phase stator power winding is directly connected to the AC grid. Whereas the converter supplies the control winding. The novelty lies in using the 5-phase controlling winding (Figure 2 and Figure 4).

Furthermore, the stator windings have been designed in a specific manner to mitigate the direct electromagnetic coupling between the power and control windings of the machine. Because in the proposed design the power winding has the number of pole pairs equal to 1 and the 5-phase control winding has the number of pole pairs equal to 3 the third harmonic of the flux linkage distribution of the power winding can couple electromagnetically with the first harmonic of the control. Thus the 3-phase power winding has a double layer winding structure with 5 coil span. The full winding function approach has been presented in [27].

In this study the finite analysis model in Ansys Maxwell has been developed. The chosen simulation results has been presented in the Figure 5. The maximum airgpap flux density under the nominal load is aprox. 1 Trms. In Figure 5d, the flux density over the airgap circuit length is presented. The flux density curve is symmetrical, as expected and desired. The maximum value of the flux density is in the rotor core and is aporx 1.8 T. In the next section, the simulation results of no-load and load are compared to the test bench results.
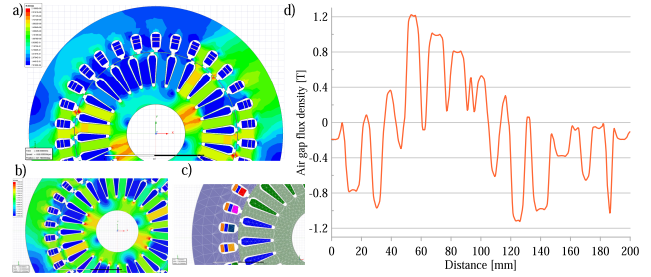
FIGURE 5. The simulation results of the BLDFIG: a) The FEA under the nominal load conditions, b) The FEA under the no-load condition, c) the mesh results, d) The flux density in airgap under the nominal load.

IV. VECTOR CONTROL OF THE STAND-ALONE 5-PHASE GENERATOR

The control system shown in Figure 6 uses a reference frame aligned with the stator PW flux vector ($\Psi_{1d} = |\Psi_1|$, $\Psi_{1q} = 0$) and is dedicated to a generator stand-alone mode application. It was assumed that the generator was not controlled by using the second mathematical plane in the control system used. The components of the voltage vector of the control winding are zero ($u_{2x} = u_{2y} = 0$). For stand-alone operation, the equivalent stator power winding magnetizing current i_{m1} is supplied entirely from the stator control winding by the coupling rotor circuit. Aligning the d–q axis of the reference frame on the stator power winding flux vector and usign (5) gives

$$i_{1d} = \frac{L_{m1}}{L_{1(1)}}(i_{m1} - i_{rd}), \quad i_{1q} = -\frac{L_{m1}}{L_{1(1)}}i_{rq} \tag{19}$$

with a constant power winding flux value, the second term of equation (2) assumes a small value. The component of the rotor current in the d-axis can adjust the excitation current i_{m1}. The dynamics of changes in the magnetizing current assume the relationships (19) and that ($\Psi_1 = L_{m1}i_{m1}$) can be written in as [28]:

$$\tau_{ms}\frac{di_{m1}}{d\tau} + i_{m1} = i_{rd} + \frac{1}{R_{1(1)}}\frac{L_{1(1)}}{L_{m1}}u_{1d} \tag{20}$$

where τ_{ms} is time constant of power winding equal $L_{1(1)}/R_{s(1)}$. The rotor current components i_{rd}, i_{irq} can be controlled indirectly by controlling the current components i_{2s}, i_{2q} in the generator control winding according to the relationship:

$$i_{rd} = -\frac{1}{\sigma_{1r}}\left(\frac{L_{m1}^2}{L_{1(1)}}i_{m1} + L_{m2}i_{2d}\right) \quad i_{rq} = -\frac{L_{m2}}{L_{r(1)}\sigma_{1r}}i_{2q} \tag{21}$$

The control winding current dynamic using (19) and (20) and taking assumptions that rotor resistance is close to zero ($R_{r(1)} \approx 0$) are defined in simplified form as follows:

$$u_{2d} = R_{2(1)}i_{2d} + L_{2(1)}\sigma_2\frac{di_{2d}}{d\tau} + \left\{\gamma_1\frac{di_{m1}}{d\tau} + \gamma_2 i_{2q} + \gamma_3 i_{1q}\right\} \tag{22}$$
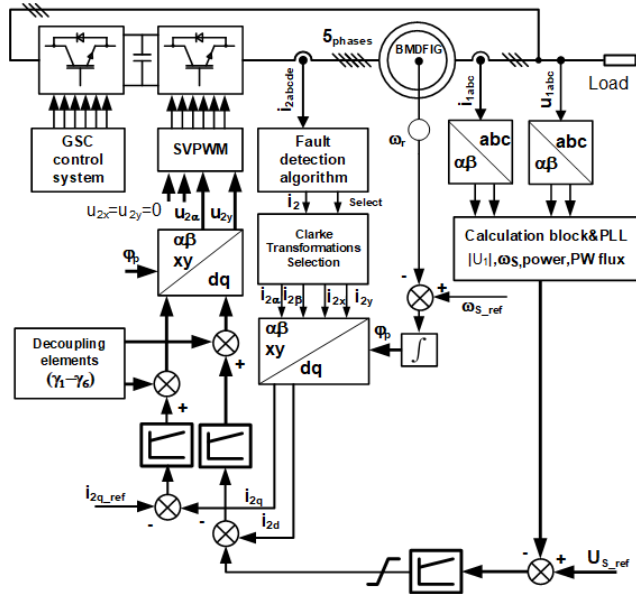
FIGURE 6. Control scheme for the BMDFIG for the 1st mathematical plane.

$$u_{2q} = R_{2(1)}i_{2q} + L_{2(1)}\sigma_2\frac{di_{2q}}{d\tau} + \{\gamma_4 i_{m1} + \gamma_5 i_{2d} + \gamma_6 i_{1d}\}$$

(23)

where σ_{1r}, σ_1, and σ_2 are variables dependent on the machine parameters and are defined in the Appendix The complete form of the equations is included in the Appendix. Equations (22)-(23) show that changing the values of the components of the control winding supply voltage vector affects the dynamics of the control winding current. These equations contain additional terms($\gamma_1 - \gamma_6$), coupling both control paths. Decoupling elements in the control paths are necessary for the proper operation of the control system, especially in dynamic states of generator operation.

The voltage regulation system consists of two control loops in a cascade structure. The external loop in the control path of the d-axis component of the CW current i_2 is responsible for control the excitation of the generator. The value of the CW current component i_{2q} in the q-axis is set to zero. To transform the components of the voltage vector set in the CW circuit, the slip angle calculated on the basis of

$$\theta_{slip} = \theta_e - \theta_r = \int \omega_e^* dt - \theta_r$$

(24)

where θ_r is measured using an incremental encoder. Using $\alpha - \beta$ components, the PW flux is obtained from the power winding voltages and currents as

$$\Psi_{1\alpha} = \int (u_{1\alpha} - R_{1(1)}i_{1\alpha})dt$$

$$\Psi_{1\beta} = \int (u_{1\beta} - R_{1(1)}i_{1\beta})dt$$

(25)

Control systems for multiphase machines in situations of emergency shutdown of one or more phases are known and described in the literature [29], [30]. Conventional control

in the case of five-phase systems in a postfault can be achieved by appropriately modifying the current set and using controllers that can cope with noncircular current reference trajectories. The key is to control the current components in such a way as to ensure the possibly circular trajectory of the rotating flux in the magnetic circuit of the machine. In the normal operating state of the generator, the currents in the control winding for the control algorithm are transformed into an orthogonal system using the Clarke transformation for five-phase systems in the form (27) (Appendix). When one of the phases is deactivated, the generator becomes an asymmetric machine, therefore the standard Clarke transformation does not ensure the correct transformation. The spatial asymmetry of the four healthy control windings leads to a system of equations with time-variant terms, which are challenging to handle and control. To maintain the symmetry of the equations before the pre-fault, in the situation after the post-fault, the presented functional control algorithm uses a modified Clark transformation in the form (28) (Appendix). This transformation modification and control approach was proposed and detailed in [31]. The fault detection algorithm functional block based on the measured value of the control winding currents, the algorithm determines the phase of the control winding where the current decay occurred and then selects the required form of the Clarke transformation. When one of the five phases of the generator control winding is deactivated, the current values in the remaining healthy phases must be increased to maintain the magnetomotive force [32].

For this reason, it is necessary to limit the electromagnetic torque on the generator and, therefore, the power transmitted to the load. This is done to guarantee the required voltage amplitude value ($|u_1| = const.$) at the terminals of the power winding of a generator operating in stand-alone mode. The value of the CW current component in emergency operation mode must be limited because it may exceed the permissible value. The failure mode determines the value of the current component limitation in the d-axis based on information on how many phases are deactivated.

V. LABORATORY TESTS
A. EXPERIMENTAL SETUP
Experimental results were carried out in the 500 W generator system. The parameters and data of the generator are reported in the Appendix. The control system with the Field-oriented control from Figure 6 was implemented in a DSP board with a Sharc ADSP21363 floating-point signal processor and Altera Cyclone II FPGA. The PWM switching frequency was 3.3 kHz. The code of the algorithm was not optimized for a DSP processor. The interruption time was set at 150 μs. The experimental stand contains the BMDFIG connected to the squire cage induction machine. The PW of BMDFIG was connected to the external variable load. The 5-phase CW was connected to the bi-directional voltage source converter of our prototype design. The mechanical speed of the generator shaft is adjusted by a universal commercial drive control unit.
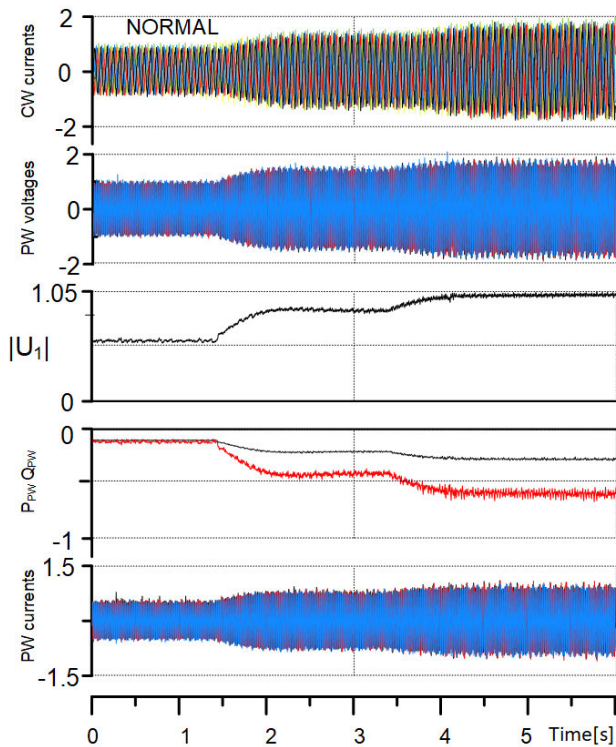
FIGURE 7. Experimental results under voltage PW reference steps.

FIGURE 8. Control winding current in the steady state condition. Oscilloscope measurements and comparison of the measurements and FEA simulations.

The rotor position angle and speed of the generator rotor are measured using an incremental encoder with a resolution of 720 pulses per rev.

B. DYNAMICAL STATE OF THE BMDFIG SYSTEM

Two sets of tests are performed to evaluate the performance of the generator. The first set of tests focuses on the dynamic states of the generator under normal operating conditions. The second set of tests is carried out to evaluate the generator's performance under emergency conditions. The generator control system is tested during normal operating conditions while varying the reference voltage, rotor speed, and load. During the first test, the turbine is operated with a continuous load and at a constant speed below the synchronous speed (ω_r = 0.5 per unit (p.u.)). The test is conducted at a given wind speed, with the reference voltage varying in three steps from 50% to 100% **Us**. The turbine's rotation speed is regulated to an optimal level to ensure that it captures maximum power from the wind.

The generator is magnetized from the CW side, and the output voltage at the PW terminals is controlled at a constant frequency and magnitude. Experimental results are shown in Figure 7 and have been compared with the finite elements analysis (FEA) silmulation results (Figure 8).

The second test is conducted at a constant rotor speed (ω_r = 0.5 p.u.) and a continuous set reference voltage value in the control algorithm. Step load changes of 100 W to 500 W are forced at the PW side. The experimental results are illus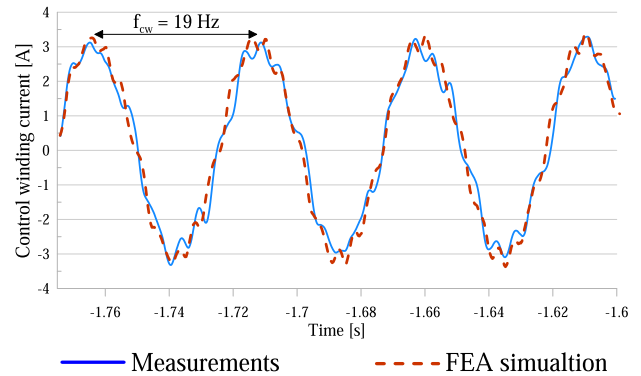trated in Fig. 9. The algorithm maintains a stable voltage and responds rapidly to changes in the output load. The vector voltage changes around 0.02 p.u. maximum.

During the next test (Figure 10), a machine was loaded with a constant value load of 500 W while its rotor speed changed between under-synchronous and over-synchronous speeds in the range of 0.5 to 1. The external drive motor was used to force the generator shaft's speed change, with an increment of approximately 500 rev/min (0.5 p.u). The generator control system functioned properly within the allowable range of changes in rotor rotational speed. The voltage at the machine terminals remained at the voltage reference value of the governor.

C. PERFORMANCE UNDER PHASES FAILURE STATES OF BMDFIG

The second stage of laboratory testing was conducted under faulty conditions and with a three phase symmetrical load. If one or two phases fail on the CW side, the system will not shut down, but it will affect the generator's operation in a stand-alone configuration. Therefore, it is essential to test the control system's behavior under one-phase and two-phase power on CW side failure. Identical tests as under normal conditions were conducted - voltage regulation steps under the constant load (Figure 11) and at constant load under the speed change (Figure 12). Overall, the reliability tests indicate that the proposed approach enables fault-tolerant performance of the generation system in the event of a single-phase control winding failure. A comparison of the results of the normal condition tests with those of the present study reveals a small increase in the magnitude of torque fluctuations as well as active power. Nevertheless, this fluctuation does not exert a significant influence on the energy generation system.

Figure 13 shows the harmonic content in the voltage induced at the PW winding terminals for the rated load of the machines at sub-synchronous (500 rev/min) and super-synchronous (1000 rev/min) rotor speeds. The fundamental output voltage harmonic is 50Hz with numerous higher-order harmonics. The presented results concern normal (NORMAL) and emergency operating conditions in the
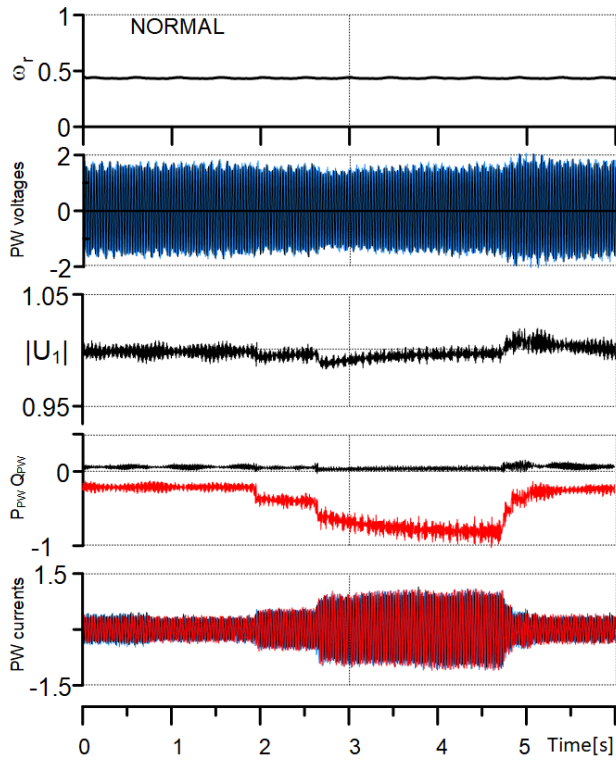
FIGURE 9. Experimental results under different load condition ((ω_r = 0.5 p.u).
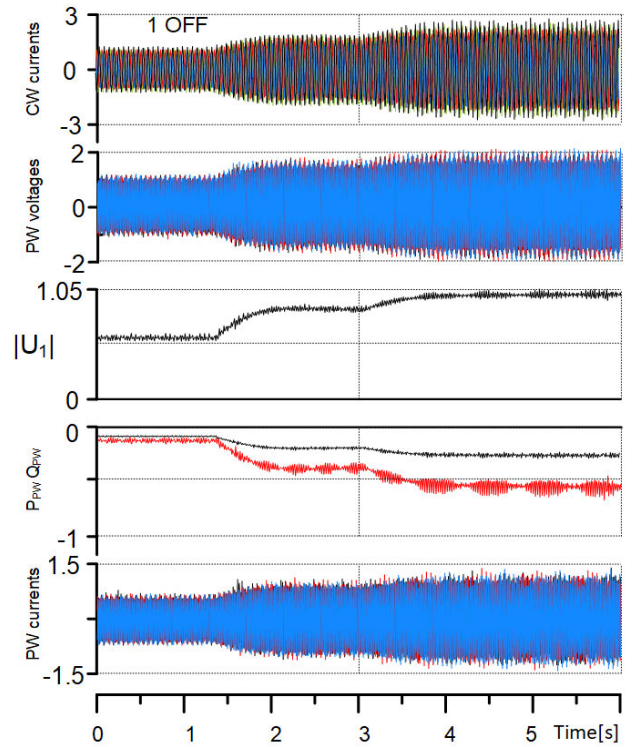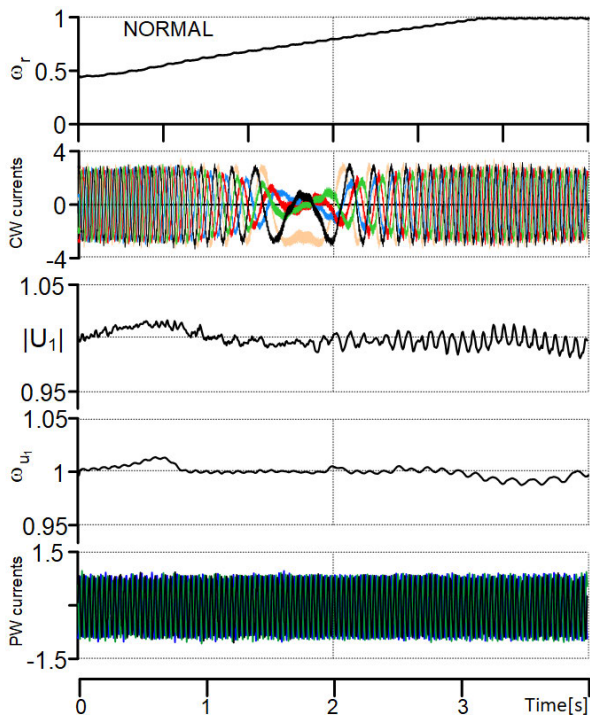

FIGURE 10. Experimental results under rotor speed variation (ω_r = 0.5-1 p.u) at normal condition.

FIGURE 11. Experimental results under voltage PW reference steps with 1 phase deactivated.
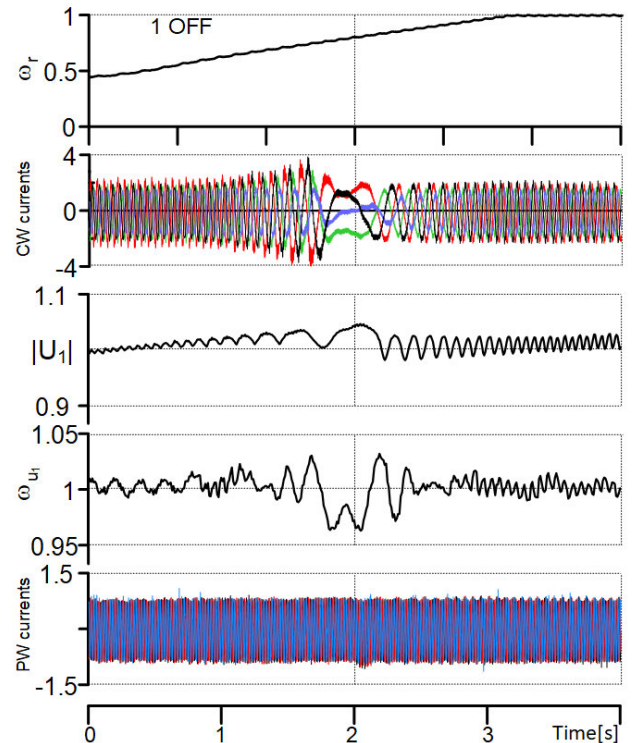

FIGURE 12. Experimental results under rotor speed variation with 1 phase deactivated.

event of deactivation of one of the phases (1 OFF) of the control winding. The total harmonic distortion rates of PW

voltage under nominal load for the extreme values of the allowable range rotational speed change are 14.2 % for
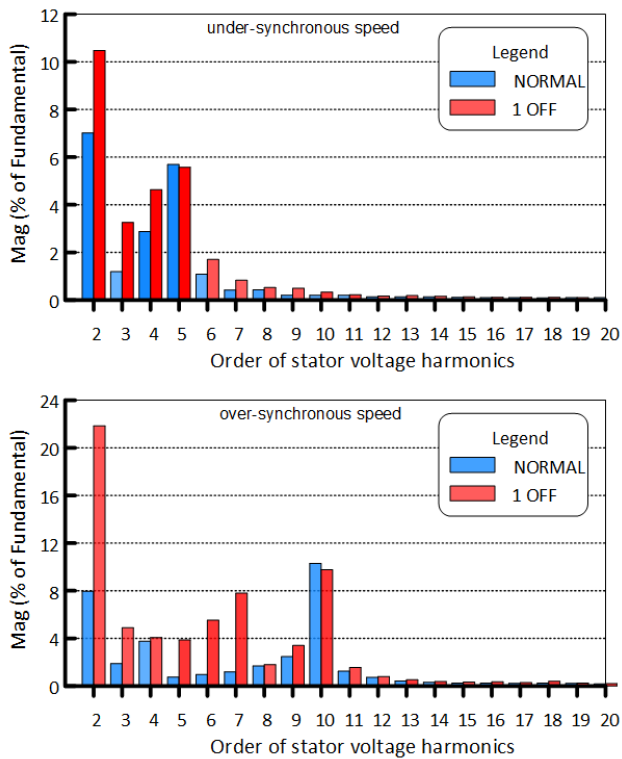
FIGURE 13. Spectrum of voltage harmonics induced in the stator power winding for different operating states of the generator:
a) under-synchronous rotor speed, b) over-synchronous rotor speed.

TABLE 1. BDFIG generator system comparison.

Generator System Comparison		
Feature	Classic BDFIG	BMDFIG
Field-oriented Control	YES [33]	YES (tested)
Direct-Voltage Control	YES [34], [35]	YES (tested)
Nonlinear Control	YES [36], [37]	YES (tested)
Phase rotor current	Normal	Lower than BDFIG
1-phase fault tolerant	Not possible	Possible (tested)
2-phase fault tolerant	Not possible	Possible (tested)

normal conditions and 24.2% for one phase deactivated. In the presented voltage harmonic distribution spectrum, there are both even harmonics. The oscillation of the output voltage amplitude manifests 2nd order harmonics. When the generator operates at super-synchronous speed, a 10th-order harmonic appears in the output voltage with a value of approximately 10% of the fundamental component, below 1% for sub-synchronous speed. The harmonic content depends on the generator's current operating point and results from the double transformation of the magnetic field between the three working windings of the generator. This is especially visible when one of the phases supplying the CW winding is deactivated (1 OFF).

VI. CONCLUSION
In this paper, the voltage controller for stand-alone mode configuration dedicated to the BMDFIG system has been
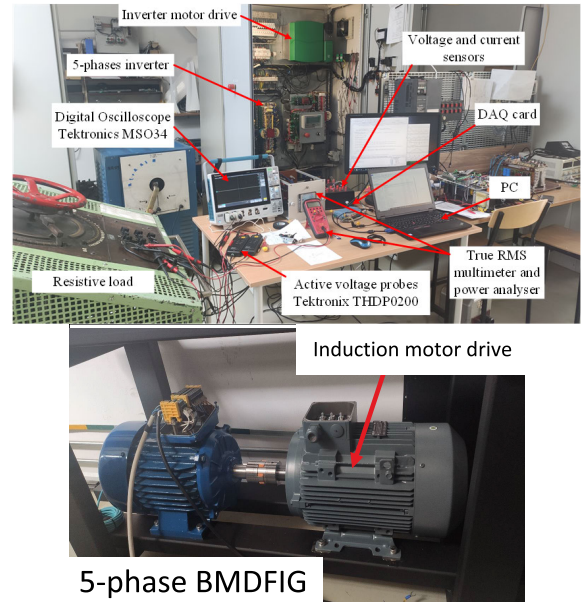

FIGURE 14. Laboratory drive shaft with prototype BMDFIG and its bi-directional power converter.

presented and elaborated. The power generation system consists of a novel construction with multi-phase control winding with dedicated multiphase power supply and traditional three-phase power winding. The prototype of the power generating system has been verified by simulating and testing on the laboratory test bench. Finally, the prototype was adapted to the different energy management scenarios such as speed and load changes, inverter or winding branch failure. A comparison of the simulation results with the experimental results has been performed. No-load and varying load dynamic off-grid tests were performed. Moreover, the laboratory prototype of the BMDFIG was used to investigate its fault tolerance performance. These tests were performed by appropriately controlling the BMDFIG when a phase was deactivated on the generator or converter control side. A direct comparison of various DFIG generator system designs has been provided in Table 1. The results presented in this paper will provide a basis for future research in the field of multiphase power generation systems.

APPENDIX
The laboratory stand's photo is displayed in Figure 14. The drive system comprises a 5 kW squirrel-cage motor and an 500 W brushless multiphase doubly-fed generator with an incremental encoder. The drive motor is powered by a commercial voltage source inverter (VSI). In contrast, the generator is supplied by a prototype five-phase bidirectional voltage source converter with complete access to software and hardware levels.

$$u_{2d} = R_{2(2)}i_{2d} + L_{2(2)}\sigma_2 \frac{di_{2d}}{d\tau} + \gamma_1 \frac{di_{m1}}{d\tau} + \gamma_2 i_{2q} + \gamma_3 i_{1q}$$

$$u_{2q} = R_{2(2)}i_{2q} + L_{2(2)}\sigma_2 \frac{di_{2q}}{d\tau} + \gamma_4 i_{m1} + \gamma_5 i_{2d} + \gamma_6 i_{1d}$$

$$(26)$$

TABLE 2. Main Specifications Of The Studied BMDFIG prototype.

Parameter	Machine	
Rated Power	Pn	0.5 kW
PW Voltage	Un	140V
PW Current	In	2A
Natural synchronous speed	nn	750 rpm
Speed range	nr	500-1000 rpm
PW / CW Pair poles	p_1/p_2	1 / 3
PW / CW phases	mPW/mCW	3 / 5
Stator slots	Qs	30
Rotor slots	Qr	24
Rotor loops per pole	Rl	3
Outer stator diameter	Dso	205
Inner stator diameter	Dsi	133.33
Airgap length	lg	0.3 mm
Axial length	ls	155 mm
PW Inductance	$L_{1(1)}$	0.08 H
PW Resistance	$R_{2(1)}$	1.159 Ω
CW Inductance	$L_{2(1)}$	0.03 H
CW Resistance	$R_{2(1)}$	12.37 Ω
RW Resistance	$R_{r(1)}$	0.53 Ω

where

$$\gamma_1 = -\frac{L_{m2}L_{m1}^2}{\sigma_{1r}L_{r(1)}L_{1(1)}} \quad \gamma_2 = \left(\omega_{sp1}\frac{L_{m2}^2}{L_{r(1)}\sigma_{1r}} - \omega_{sp2}L_{2(2)}\right)$$

$$\gamma_3 = -\frac{L_{m2}L_{1(1)}}{L_{m1}}\left(\omega_{sp1} - \omega_{sp2}\right)$$

$$\gamma_4 = \left(\omega_{sp2}L_{m2} - \frac{\sigma_{1r}L_{1(1)}L_{m2} - L_{m2}L_{m1}^2}{L_{r(1)}\sigma_{1r}L_{1(1)}}\omega_{sp1}\right)$$

$$\gamma_5 = -\left(\omega_{sp1}\frac{L_{m2}^2}{L_{r(1)}\sigma_{1r}} - \omega_{sp2}L_{2(1)}\right)$$

$$\gamma_6 = \frac{L_{1(1)}}{L_{m1}}\left(\omega_{sp2}L_{m2} - \frac{L_{m2}}{L_{r(1)}}\omega_{sp1}\right)$$

$$\sigma_{1r} = \left(1 - \frac{L_{m1}^2}{L_{r(1)}L_{1(1)}}\right) \quad \sigma_2 = \left(1 - \frac{L_{m2}^2}{L_{2(1)}L_{r(1)}\sigma_{1r}}\right)$$

The BMDFIG nominal parameters are presented in Table 2.

$$
\begin{bmatrix} i_\alpha \\ i_\beta \\ i_x \\ i_y \end{bmatrix}
= \frac{2}{5}
\begin{bmatrix}
1 & \cos(\vartheta) & \cos(2\vartheta) & \cos(2\vartheta) & \cos(\vartheta) \\
0 & \sin(\vartheta) & \sin(2\vartheta) & -\sin(2\vartheta) & -\sin(\vartheta) \\
1 & \cos(2\vartheta) & \cos(4\vartheta) & \cos(4\vartheta) & \cos(2\vartheta) \\
0 & \sin(2\vartheta) & \sin(4\vartheta) & -\sin(4\vartheta) & -\sin(2\vartheta)
\end{bmatrix}
\begin{bmatrix} i_a \\ i_b \\ i_c \\ i_d \\ i_e \end{bmatrix}
\tag{27}
$$

$$
\begin{bmatrix} i_\alpha \\ i_\beta \\ i_x \\ i_y \end{bmatrix}
= \frac{2}{5}
\begin{bmatrix}
a_{11} & a_{12} & a_{13} & a_{14} \\
\sin(\vartheta) & \sin(2\vartheta) & \sin(3\vartheta) & \sin(4\vartheta) \\
\sin(2\vartheta) & \sin(4\vartheta) & \sin(6\vartheta) & \sin(8\vartheta) \\
1 & 1 & 1 & 1
\end{bmatrix}
\begin{bmatrix} i_b \\ i_c \\ i_d \\ i_e \end{bmatrix}
\tag{28}
$$

where

$$a_{11} = cos(\vartheta) - 1; \qquad a_{12} = cos(2\vartheta) - 1$$
$$a_{13} = cos(3\vartheta) - 1; \qquad a_{14} = cos(4\vartheta) - 1$$

REFERENCES

[1] M. G. Jovanovic, R. E. Betz, and J. Yu, "The use of doubly fed reluctance machines for large pumps and wind turbines," *IEEE Trans. Ind. Appl.*, vol. 38, no. 6, pp. 1508–1516, Nov. 2002.

[2] T. D. Strous, H. Polinder, and J. A. Ferreira, "Brushless doubly-fed induction machines for wind turbines: Developments and research challenges," *IET Electr. Power Appl.*, vol. 11, no. 6, pp. 991–1000, Jul. 2017.

[3] Y. Liu, M. G. Hussien, W. Xu, S. Shao, and E. M. Rashad, "Recent advances of control technologies for brushless doubly-fed generators," *IEEE Access*, vol. 9, pp. 123324–123347, 2021.

[4] W. Łyskawiński, K. Kowalski, and R. M. Wojciechowski, "Experimental assessment of suitability of darrieus and savonius turbines for obtaining wind energy from passing vehicles," *Energies*, vol. 17, no. 7, p. 1558, Mar. 2024. [Online]. Available: https://www.mdpi.com/1996-1073/17/7/1558/htm

[5] P. Han, M. Cheng, S. Ademi, and M. G. Jovanovic, "Brushless doubly-fed machines: Opportunities and challenges," *Chin. J. Electr. Eng.*, vol. 4, no. 2, pp. 1–17, Jun. 2018. [Online]. Available: https://ieeexplore.ieee.org/document/8409345

[6] X. Wang, J. Zhao, R. Guo, and Z. Jiang, "Research on design of brushless doubly fed generator," in *Proc. IEEE Power Eng. Autom. Conf. (PEAM)*, vol. 1, Sep. 2011, pp. 46–49.

[7] W. Ullah, F. Khan, and S. Hussain, "A comparative study of dual stator with novel dual rotor permanent magnet flux switching generator for counter rotating wind turbine applications," *IEEE Access*, vol. 10, pp. 8243–8261, 2022.

[8] Y. Wang, S. L. Ho, W. N. Fu, and J. X. Shen, "A novel brushless doubly fed generator for wind power generation," *IEEE Trans. Magn.*, vol. 48, no. 11, pp. 4172–4175, Nov. 2012. [Online]. Available: http://ieeexplore.ieee.org/document/6332704/

[9] F. Zhang, S. Yu, Y. Wang, S. Jin, and M. G. Jovanovic, "Design and performance comparisons of brushless doubly fed generators with different rotor structures," *IEEE Trans. Ind. Electron.*, vol. 66, no. 1, pp. 631–640, Jan. 2019.

[10] M. E. Achkar, R. Mbayed, G. Salloum, N. Patin, and E. Monmasson, "Voltage control of a stand-alone doubly fed induction generator," *IEEE Trans. Ind. Electron.*, vol. 66, no. 1, pp. 762–771, Jan. 2019. [Online]. Available: https://ieeexplore.ieee.org/document/8415745/

[11] A. M. Knight, R. E. Betz, and D. G. Dorrell, "Design and analysis of brushless doubly fed reluctance machines," *IEEE Trans. Ind. Appl.*, vol. 49, no. 1, pp. 50–58, Jan. 2013.

[12] O. Sadeghian, S. Tohidi, B. Mohammadi-Ivatloo, and F. Mohammadi, "A comprehensive review on brushless doubly-fed reluctance machine," *Sustainability*, vol. 13, no. 2, p. 842, Jan. 2021.

[13] H. Liu, Y. Zhang, F. Zhang, S. Jin, H. Zhang, and H. Nian, "Design and performance analysis of dual-stator brushless doubly-fed machine with cage-barrier rotor," *IEEE Trans. Energy Convers.*, vol. 34, no. 3, pp. 1347–1357, Sep. 2019. [Online]. Available: https://ieeexplore.ieee.org/document/8601368/

[14] S. Yu, Y. Zhang, C. Chen, F. Zhang, and H. Nian, "Loss estimation of brushless doubly-fed generator with hybrid rotor considering multiple influence factors," *IEEE Access*, vol. 8, pp. 60043–60051, 2020.

[15] P. Han, M. Cheng, X. Wei, and Y. Jiang, "Steady-state characteristics of the dual-stator brushless doubly fed induction generator," *IEEE Trans. Ind. Electron.*, vol. 65, no. 1, pp. 200–210, Jan. 2018. [Online]. Available: http://ieeexplore.ieee.org/document/7953581/

[16] I. Boldea, L. N. Tutelea, C. Wu, F. Blaabjerg, Y. Liu, M. G. Hussien, and W. Xu, "Fractional kVA rating PWM converter doubly fed variable speed electric generator systems: An overview in 2020," *IEEE Access*, vol. 9, pp. 117957–117968, 2021.

[17] Z. Li, X. Wang, M. Kong, and X. Chen, "Bidirectional harmonic current control of brushless doubly fed motor drive system based on a fractional unidirectional converter under a weak grid," *IEEE Access*, vol. 9, pp. 19926–19938, 2021.

[18] A. Kumar, P. K. Sadhu, and J. Singh, "A technological review of wind power generation," *IOP Conf. Ser., Mater. Sci. Eng.*, vol. 691, no. 1, Nov. 2019, Art. no. 012017. [Online]. Available: https://iopscience.iop.org/article/10.1088/1757-899X/691/1/012017

[19] J. Hu, H. Yuan, and X. Yuan, "Modeling of DFIG-based WTs for small-signal stability analysis in DVC timescale in power electronized power systems," *IEEE Trans. Energy Convers.*, vol. 32, no. 3, pp. 1151–1165, Sep. 2017. [Online]. Available: http://ieeexplore.ieee.org/document/7921439/

[20] R. McKenna, P. O. V. D. Leye, and W. Fichtner, "Key challenges and prospects for large wind turbines," *Renew. Sustain. Energy Rev.*, vol. 53, pp. 1212–1221, Jan. 2016.

[21] L. Zhu, F. Zhang, S. Jin, S. Ademi, X. Su, and W. Cao, "Optimized power error comparison strategy for direct power control of the open-winding brushless doubly fed wind power generator," *IEEE Trans. Sustain. Energy*, vol. 10, no. 4, pp. 2005–2014, Oct. 2019.

[22] O. M. E. Mohammed, W. Xu, Y. Liu, and F. Blaabjerg, "An improved control method for standalone brushless doubly fed induction generator under unbalanced and nonlinear loads using dual-resonant controller," *IEEE Trans. Ind. Electron.*, vol. 68, no. 7, pp. 5594–5605, Jul. 2021. [Online]. Available: https://ieeexplore.ieee.org/document/9097376/

[23] Y. Liu, Y. Zhang, W. Xu, M. Zhang, W. Pan, J. Rodriguez, and I. Boldea, "Improved efficiency optimization control for brushless doubly fed induction generator–DC system by regulating stator frequency," *IEEE Trans. Power Electron.*, vol. 38, no. 3, pp. 3624–3639, Mar. 2023.

[24] R. Ryndzionek, K. Blecharz, F. Kutt, M. Michna, and G. Kostro, "Fault-tolerant performance of the novel five-phase doubly-fed induction generator," *IEEE Access*, vol. 10, pp. 59350–59358, 2022.

[25] A. Oraee, R. Mcmahon, E. Abdi, S. Abdi, and S. Ademi, "Influence of pole-pair combinations on the characteristics of the brushless doubly fed induction generator," *IEEE Trans. Energy Convers.*, vol. 35, no. 3, pp. 1151–1159, Sep. 2020. [Online]. Available: https://ieeexplore.ieee.org/document/9044321/

[26] P. C. Roberts, R. A. Mcmahon, P. J. Tavner, J. M. Maciejowski, and T. J. Flack, "Equivalent circuit for the brushless doubly fed machine (BDFM) including parameter estimation and experimental verification," *IEE Proc. Electr. Power Appl.*, vol. 152, no. 4, p. 933, 2005.

[27] R. Ryndzionek, K. Blecharz, F. Kutt, G. Kostro, M. Michna, and M. Morawiec, "Winding function approach based design of novel five-phase brushless doubly fed induction generator," in *Proc. Int. Conf. Clean Electr. Power (ICCEP)*, Jun. 2023, pp. 316–321.

[28] R. Pena, R. Cardenas, J. Proboste, G. Asher, and J. Clare, "Sensorless control of doubly-fed induction generators using a rotor-current-based MRAS observer," *IEEE Trans. Ind. Electron.*, vol. 55, no. 1, pp. 330–339, Jan. 2008.

[29] B. Chikondra, A. G. Yepes, O. Al Zaabi, K. Al Hosani, J. D. Gandoy, and R. K. Behera, "Open-phase fault-tolerant DTC technique for three-level NPC VSI-fed five-phase induction motor drives," *IEEE J. Emerg. Sel. Topics Power Electron.*, vol. 11, no. 2, pp. 2114–2125, Apr. 2023.

[30] M. Medina-Sánchez, A. G. Yepes, Ó. López, and J. Doval-Gandoy, "Assessment and exploitation of the minimum current harmonic distortion under overmodulation in five-phase induction motor drives," *IEEE Trans. Power Electron.*, vol. 38, no. 4, pp. 4289–4305, Apr. 2023.

[31] H. Guzman, M. J. Duran, F. Barrero, B. Bogado, and S. Toral, "Speed control of five-phase induction motors with integrated open-phase fault operation using model-based predictive current control techniques," *IEEE Trans. Ind. Electron.*, vol. 61, no. 9, pp. 4474–4484, Sep. 2014.

[32] J.-R. Fu and T. A. Lipo, "Disturbance-free operation of a multiphase current-regulated motor drive with an opened phase," *IEEE Trans. Ind. Appl.*, vol. 30, no. 5, pp. 1267–1274, Mar. 1994.

[33] M. Jovanović, S. Ademi, and R. Binns, "Sensorless variable speed operation of doubly-fed reluctance wind generators," *IET Renew. Power Gener.*, vol. 14, no. 15, pp. 2810–2819, Nov. 2020, doi: 10.1049/iet-rpg.2020.0021.

[34] K. Yu, W. Xu, Y. Liu, and S. Zhang, "Improved sensorless direct voltage control of standalone doubly-fed induction generator feeding nonlinear loads," in *Proc. 21st Int. Conf. Electr. Mach. Syst. (ICEMS)*, Oct. 2018, pp. 1674–1679.

[35] Y. Liu, W. Xu, F. Xiong, and F. Blaabjerg, "Sensorless direct voltage control of the stand-alone brushless doubly-fed generator," in *Proc. 20th Int. Conf. Electr. Mach. Syst. (ICEMS)*, Aug. 2017, pp. 1–6. [Online]. Available: https://vbn.aau.dk/en/publications/sensorless-direct-voltage-control-of-the-stand-alone-brushless-do

[36] H. M. Hesar, X. Liang, H. A. Zarchi, H. Chenarani, and A. Khazaee, "High-efficient nonlinear control for brushless doubly-fed induction machines," *IEEE Trans. Energy Convers.*, vol. 38, no. 2, pp. 1442–1451, Jun. 2023.

[37] O. Moussa, R. Abdessemed, S. Benaggoune, and H. Benguesmia, "Sliding mode control of a grid-connected brushless doubly fed induction generator," *Eur. J. Electr. Eng.*, vol. 21, no. 5, pp. 421–430, Nov. 2019.

KRZYSZTOF BLECHARZ received the M.Sc. degree in electrical engineering from Czestochowa University of Technology, Czestochowa, Poland, in 2002, and the Ph.D. degree in electrical drives from the Gdańsk University of Technology, Gdańsk, Poland, in 2008. Since 2008, he has been an Adjunct Professor with Gdańsk University of Technology. He is the author of over 30 articles, four Polish patents, and a participant in many research projects as a designer or a researcher. His main scientific activities are concentrated on doubly-fed generator control systems, multiscalar models of electrical machines, sensorless control, and nonlinear control in electric drives.

ROLAND RYNDZIONEK (Senior Member, IEEE) received the M.Sc. degree in electrical engineering from Gdańsk University of Technology (Gdańsk Tech), Gdańsk, Poland, in 2010, the M.Sc. degree in electrical engineering from INP ENSEEIHT, Toulouse, France, in 2012, and the Ph.D. degree in electrical engineering from Gdańsk Tech and INP, in 2015. From 2015 to 2017, he was a Postdoctoral Research Engineer with SuperGrid Institute, Lyon, France. Since 2017, he has been with Gdańsk Tech (formerly GUT), where he is currently an Assistant Professor. His scientific and research interests include the development of piezoelectric motors for embedded applications, designing of the mechatronic structures, and power converters.

FILIP KUTT was born in Gdańsk, Poland. He received the M.Sc. and Ph.D. degrees in electrical engineering from Gdańsk University of Technology (GUT), Poland, in 2007 and 2013, respectively. He is an Assistant Professor with the Department of Power Electronics and Electrical Machines, Faculty of Electrical and Control Engineering, GUT. He has been with GUT, since 2007. He is participating in several projects focusing on the development of innovative multiphase electromechanical energy converters. His main scientific and research interests include a wide spectrum of mathematical modeling of electrical machines using analytical modeling and FEM-based computations.

• • •